IEICE TRANS. ELECTRON., VOL.E102–C, NO.1 JANUARY 2019

PAPER Special Section on Recent Progress in Electromagnetic Theory and Its Application

A Fundamental Study on Vehicle Detection in Flooded Urban Area Using Quad-Polarimetric SAR Data

Takanori ISHIKURO[†a)], ***Student Member***, **Ryoichi SATO**[††b)], ***Member***, **Yoshio YAMAGUCHI**[†††c)], ***Fellow***, ***and*** **Hiroyoshi YAMADA**[†††d)], ***Senior Member***

SUMMARY In this paper, we propose a simple algorithm for detecting a vehicle trapped in flooded urban area by using quad-polarimetric SAR data. The four-component scattering power decomposition and phase difference of HH-VV co-pol ratio are effectively used in the proposed algorithm. Here we carry out polarimetric scattering measurement for a scaled vehicle model surrounded by two buildings model in an anechoic chamber, to acquire the quad-polarimetric SAR data. It is confirmed from the results of the image analysis for the measured SAR data that the proposed algorithm for vehicle detection works well even under severe environment where the vehicle is set in the shadow of the building and/or the alignment of the vehicle or the buildings is obliquely oriented to direction of the radar line of sight.

key words: *radar polarimetry, vehicle detection, flooded urban area, disaster mitigation, co-pol ratio phase difference*

1. Introduction

Guerrilla rainstorm is a localized downpour of heavy rain in a short period of time. It causes a devastating disaster and it frequently occurs in recent years due to global warming phenomena. Because of unexpected and sudden downpour of rainfall, there exist victims who cannot escape from the flooded area. In case of urban flooding, people are often left and trapped inside vehicles in the valley of buildings. It is necessary to detect such vehicles as soon as possible from the rescue point of view.

High resolution synthetic aperture radar (SAR) [1] is expected to play a key role for widely monitoring flooding event. Since it works under overcast and night conditions, it provides us with the best solution to monitor the flooded area.

The most important factor in SAR observation for saving victims of urban disasters is the identification of damaged objects, e.g., correct detection of vehicle in flooded area. In observation of vehicle between buildings, radar receives scattered EM wave directly from the object as shown in Fig. 1 (a) when the incidence angle is small. In this lit region case, all the scattered EM wave is perfectly acquired as in the normal radar observation. When the incidence angle becomes large as shown in Fig. 1 (b), there exists shadow region where the radar beam is blocked and shadowed by buildings. In this case, there will be small reflected signal from object due to multiple-bouncing effect. There is a possibility to detect it by the multiple-bouncing signal. In both cases, it is necessary to identify the object correctly regardless of observation scenario. Even if the object under investigation is detected in the lit or shadow case, we have to know what kind of objects are there. It is necessary to classify the object and determine whether it is metallic or non-metallic object in the valley of buildings. The second problem is "ghost image" created by multi-bouncing scattered wave from the object, as shown in Fig. 2. Since

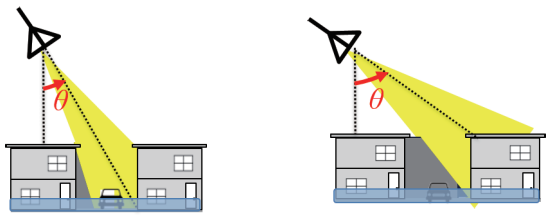

(a) Lit region (b) Shadow region

Fig. 1 Lit region and shadow region.

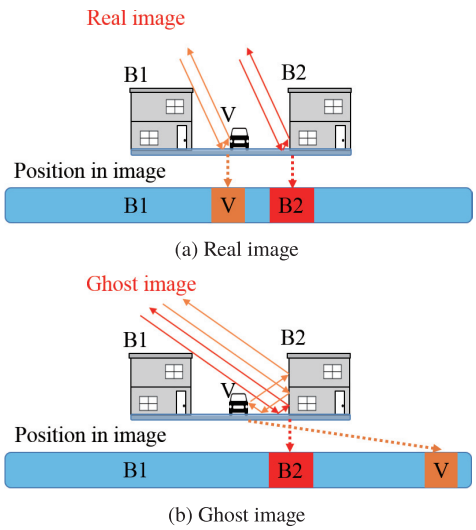

(a) Real image

(b) Ghost image

Fig. 2 Real image and ghost image.

Manuscript received March 14, 2018.
Manuscript revised July 31, 2018.

[†]The author was with the Graduate School of Science and Technology, Niigata University, Niigata-shi, 950–2181 Japan.
[††]The author is with the Faculty of Education, Niigata University, Niigata-shi, 950–2181 Japan.
[†††]The authors are with the Faculty of Engineering, Niigata University, Niigata-shi, 950–2181 Japan.
a) E-mail: ishiguro@wave.ie.niigata-u.ac.jp
b) E-mail: sator@ed.niigata-u.ac.jp
c) E-mail: yamaguch@ie.niigata-u.ac.jp
d) E-mail: yamada@ie.niigata-u.ac.jp

DOI: 10.1587/transele.E102.C.38

the path length of multi-bounce scattered wave from object is longer than that of direct scattered wave, it appears as a ghost in the slant-range direction of SAR image. For the example of Fig. 2, the double-bounce scattered wave from the vehicle (V) is depicted as the "real image" in front of the 2nd building (B2) in the lit case (Fig. 2 (a)), whereas the quadruple-bounce scattered wave from the vehicle (V) is appeared as the "ghost image" behind the 2nd building (B2) in the shadow case (Fig. 2 (b)). It is necessary to reject the ghost.

In this paper, we propose to use polarimetric techniques for identification of objects, and present a simple algorithm for detecting a vehicle in flooded area. In order to achieve this purpose, we first acquired fully polarimetric data in an anechoic chamber. The various flooding situations were modeled at Ku-band using metallic objects and concrete blocks. The data sets were used for identification of a vehicle using the four-component scattering power decomposition [2], [3] and by the phase information of HH-VV co-pol ratio [4]. Based on the analysis results, a simple vehicle detection algorithm is proposed. In the following, analysis methods are presented in Sect. 2, polarimetric measurement is described in Sect. 3, followed by experimental results in Sect. 4, and detection algorithm in Sect. 5.

2. Polarimetric Analysis Method for Vehicle Detection

To detect a vehicle trapped in flooded urban area and correctly obtain its position by using quad-polarimetric SAR data, the following two steps should be considered.

Step 1) Extraction of manmade objects region (buildings and vehicles) from whole PolSAR image.

Step 2) Recognition between the vehicle and the surrounding building in the manmade objects region extracted by **Step 1**, and judgment whether the pixels recognized as the vehicle are "real image" or "ghost image".

There are many candidates in polarimetric analysis methods [4]–[7] to execute the two steps. In this paper, we use the following two effective polarimetric analysis methods, by considering the results of our pilot study [8]. For **Step 1**, we use the four-component scattering power decomposition. For **Step 2**, we adopt phase difference of the HH-VV co-pol ratio. In this section, we briefly explain these methods.

2.1 Four-Component Scattering Power Decomposition

As solution of **Step 1**, we use the four-component scattering power decomposition to extract urban area. Let us briefly show the decomposition in the following.

By using a quad-polarimetric SAR system, we obtain the Sinclair scattering matrix $[S(HV)]$ from the scatterer as

$$[S(HV)] = \begin{bmatrix} S_{HH} & S_{HV} \\ S_{VH} & S_{VV} \end{bmatrix}, \tag{1}$$

where $S_{HV} = S_{VH}$ for monostatic case. The Pauli scattering vector $\boldsymbol{k}_P$, which is equivalent to the scattering matrix of Eq. (1), is expressed as

$$\boldsymbol{k}_P = \frac{1}{\sqrt{2}} \begin{bmatrix} S_{HH} + S_{VV} \\ S_{HH} - S_{VV} \\ 2S_{HV} \end{bmatrix}. \tag{2}$$

By using Eq. (2), the 3×3 ensemble average Coherency matrix $\langle [T] \rangle$ is obtained as

$$\langle [T] \rangle = \frac{1}{n} \sum^{n} \boldsymbol{k}_P \boldsymbol{k}_P{}^{\dagger} = \begin{bmatrix} T_{11} & T_{12} & T_{13} \\ T_{21} & T_{22} & T_{23} \\ T_{31} & T_{32} & T_{33} \end{bmatrix}, \tag{3}$$

where $\langle \cdot \rangle$ and $\dagger$ denote data averaging n pixels and complex conjugate transpose, respectively.

As shown in Fig. 3, by applying the scattering power decomposition procedure, the measured matrix $\langle [T] \rangle$ can be decomposed into fundamental physical models as surface scattering, double-bounce scattering, volume scattering and helix scattering as

$$\langle [T] \rangle = f_s [T]_{surface} + f_d [T]_{double} + f_v [T]_{vol} + f_c [T]_{helix}, \tag{4}$$

where $[T]_{surface}$, $[T]_{double}$, $[T]_{volume}$ and $[T]_{helix}$ are the expansion matrices, respectively. By determining the unknown expansion coefficients f_s, f_d, f_v, f_c, the total scattering power P_t is decomposed into the scattered powers as $P_t = P_s + P_d + P_v + P_c$, where P_s, P_d, P_v and P_c are the decomposed powers for surface scattering, double-bounce scattering, volume scattering, and helix scattering, respectively. The relationship between each decomposed power and the expansion coefficient is shown as

$$\begin{aligned} P_d &= f_d(1 + |\alpha|^2), \\ P_s &= f_s(1 + |\beta|^2), \\ P_v &= f_v, \\ P_c &= f_c, \end{aligned} \tag{5}$$

where α and β are unknown coefficients concerning the double bounce scattering and surface scattering, respectively. They are included in the corresponding expansion matrices $[T]_{double}$ and $[T]_{surface}$ (See Refs. [2], [3] in detail).

The dominant double-bounce scattering generated from the dihedral structures composed by building walls and ground surface can be utilized to extract urban areas in a SAR image.

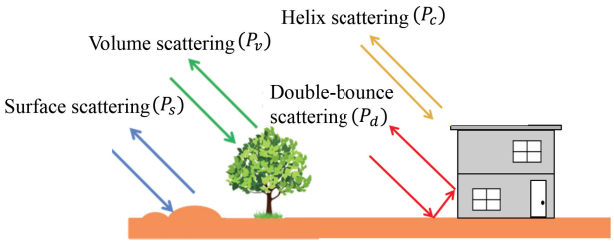

Fig. 3 Powers obtained by the scattering power decomposition.

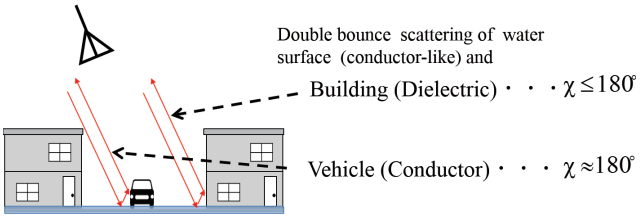

Fig. 4 χ of buildings and vehicle.

When flooding occurs in urban areas, surface of the ground is changed to that of the flooding water. The water surface may act as a conducting surface, so we expect that the double-bounce scattering after flooding is much larger than that before flooding. However, when urban building is rotated to the radar illumination direction, it may be difficult to accurately identify the urban area using the SAR data, since the effective detection indicator, strong double-bounce scattering, is not observed for this case at all, and undesired cross-polarized scattering component S_{HV} becomes large. S_{HV} sometimes degrades the detection rate of the buildings. In this paper, to mitigate the negative effect due to S_{HV} and reduce the false detection, we carry out the orientation angle compensation (OAC) [3], [9], [10] before doing the four-component decomposition.

2.2 Phase Difference of Co-Pol Ratio

It is expected that the four-component scattering power decomposition is used for accurately detecting both building and vehicle in urban area. However, the double-bounce scattering P_d obtained in the decomposition practically shows the even-bounce scattering including double-bounce, quadruple-bounce, sextuple-bounce, and so forth. Hence it is difficult to identify whether P_d from the vehicle is generated by double-bounce scattered power (real image) or by higher order multi-bounce scattered power (ghost image) (See Fig. 2 again). Therefore, we introduce an additional indicator, phase difference of co-pol (S_{HH} and S_{VV}) ratio, to distinguish the double-bounce scattering from the multi-bounce scattering.

In this paper, the phase of the HH-VV co-pol ratio, χ, is defined as

$$\chi = \angle \frac{S_{VV}}{S_{HH}}. \tag{6}$$

The OAC is again performed to the elements of both S_{HH} and S_{VV} before obtaining the phase angle χ [3], [9], [10].

We now consider the case of flooding in urban areas. As shown in Fig. 4, χ for the dihedral structure between water surface and the side surface of vehicle may become close to 180°, since the water surface may act as horizontal Perfect Electric Conductor (PEC) flat plane, and consequently the dihedral of the vehicle behaves as a PEC dihedral, whose parts are constructed by horizontal and vertical PEC planes. On the other hand, χ for the dihedral between the water surface and the sidewall of dielectric building may be smaller than 180°. The Fresnel reflection at the side surface of each object (vehicle or building) indirectly describes conductive or dielectric characteristics, respectively, and the different reflection characteristics can convert to the different behavior of χ. Hence, the behavior of χ can be used as an indicator to realize distinction between vehicle and building in such flooded urban area.

Furthermore, it is assumed for the even-bounce scattering P_d from the vehicle that χ for the double-bounce scattering in the lit case (between water surface and side surface of the vehicle) is different from that for the higher order multi-bounce scattering in the shadow case (between water surface, side surface of the vehicle, and sidewall of the dielectric building), since the number of times of the reflections at the dielectric plane may degrade the conductive behavior of χ and have strongly influence on the change of χ. Taking into account these features, the difference between χ in the lit region and χ in the shadow region may be useful as an additional indicator to distinguish the real image from the ghost image due to the higher order multi-bounce scattering in the PolSAR image.

3. Polarimetric Scattering Measurement

We do not have actual high-resolution quad-polarimetric SAR data including vehicles in flooded urban areas unfortunately, so we need to acquire the SAR data for the model of a vehicle in flooded urban areas by ourselves.

In this section, we carry out polarimetric scattering measurement for a scaled vehicle model in simplified urban valley environment, to acquire quad-polarimetric SAR data for the model.

The polarimetric scattering measurement for the vehicle model in anechoic chamber is carried out by using 4 standard horn antennas and Vector Network Analyzer (VNA) with 4-port capability at Ku band (the center frequency is 15 GHz), 4 GHz band width and 2.6 m synthetic aperture length are used in the measurement.

The model considered is composed of a small conducting rectangular parallelepiped (vehicle) surrounded by dielectric ones (buildings), as shown in Fig. 5. The size of each model is given in Figs. 5 (b) and (c). The vehicle model is made of styrene foam covered by aluminum tape. It is assumed here that the tires of the vehicle are mostly submerged below the water surface. The building model is made of concrete, and its complex permittivity at Ku-band (15 GHz) is about $3.00 - j0.45$, whose value was obtained by a measurement using a dielectric probe kit (Agilent 85070E). The buildings model is placed on a conducting plate imitating flooded water surface. The vehicle model is set at the center of the valley space between the buildings. The plate is made of thin square aluminum. The experimental setup is depicted in Fig. 6. The incidence angle θ, squint angle ϕ to the entire model (vehicle and buildings), and squint angle ξ to the vehicle are all varied (See Fig. 5 (a) and Table 1). The slant-range between the antennas and the vehicle model for $\theta = 25°$ and $\theta = 55°$ are about 1.92 m and

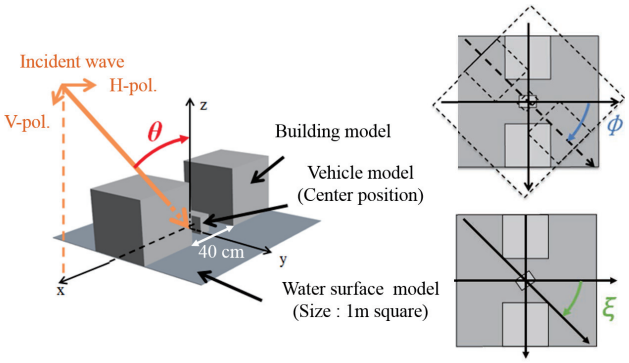

(a) Vehicle-buildings model on a conducting plate

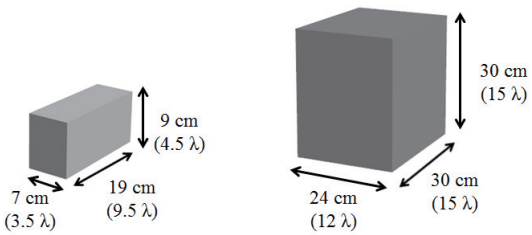

(b) Vehicle model (c) Building model

Fig. 5 Geometry of the problem.

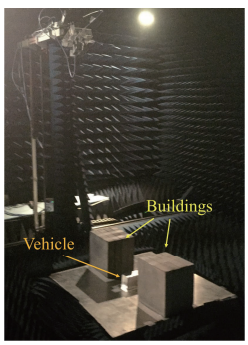

(a) Photo

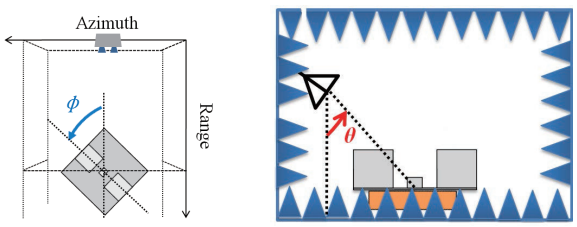

(b) Top view (c) Side view

Fig. 6 Measurement setup in anechoic chamber.

3.03 m, respectively. The measured PolSAR data description is shown in Table 2.

After multi-look processing of the acquired data, we first carry out the OAC to the coherency matrix $\langle[T]\rangle$ and the scattering matrix $[S(HV)]$, and then execute the four-component decomposition and obtain the phase of the co-pol ratio. In the next section, we shall show the results of PolSAR image analysis using these two methods.

Table 1 Measurement parameters.

Center frequency	15 GHz (Ku-band)
Band width	4.0 GHz
Incidence angle θ	25°, 55°
Squint angle (building and vehicle) ϕ	0°, 10°, 20°, 30°
Squint angle (vehicle) ξ	0°, 10°

Table 2 Measured PolSAR data description.

Mode	HH, HV, VH, VV
Pixel size	99 × 68 [pixels]
Resolution	0.010 m × 0.0375 m
Multilook size (Azimuth × Slant-range)	3 × 2 [pixels]

4. Analysis for the Measurement Data

In this section, we show the analysis results for the measured quad-polarimetric SAR data obtained in the previous section.

4.1 Power of Double-Bounce Scattering: P_d

As described before, P_d is considered as a useful indicator to extract buildings and vehicle from the whole PolSAR image, when the alignment of the building or the vehicle is almost normal to the radar illumination direction. So here we examine the behavior of P_d when the alignment is not only normal but also oblique to the radar direction.

Figures 7 and 8 show the RGB color composite images obtained by the Four-component scattering power decomposition for the lit case of $\theta = 25°$ and for the shadow case of $\theta = 55°$, respectively, where Red is assigned for P_d, Green is for P_v, and Blue is for P_s. The horizontal and vertical axes in the images indicate the azimuth and slant-range directions. The squint angle is varied as $\phi = 0°$, 10°, 20°, and 30°. Here we also show the image of the total power P_t for each case (Figs. 9 and 10). One can see from the figures that strong P_d can be clearly observed when ϕ is up to 10° for both the lit and shadow cases. Also, it is found from the comparison between the RGB (Figs. 7 and 8) and the total power images (Figs. 9 and 10) that the pixel positions with P_d dominance are almost the same as those with strong P_t. These results lead to a situation that even-bounce scattered power generated by vehicles and buildings in urban areas is relatively stable for change of the viewing condition. So P_d may be used as a reliable signature to extract pixels of the manmade objects from the whole SAR image. It is also verified from the results in the lit case of $\theta = 25°$ that P_d from the vehicle model is observed at the correct location, *i.e.* at the position in front of the building model, as shown in Fig. 2 (a). On the other hand, in the shadow case of $\theta = 55°$, we see that P_d from the vehicle is seen at the incorrect location, *i.e.* at the position behind the building, as in Fig. 2 (b). This is due to the fact that the path length of the multi-bounce (quadruple-bounce) scattering in the shadow case is longer than that of the double-bounce scattering in the lit case.

Next, we examine the phase characteristics of the HH-

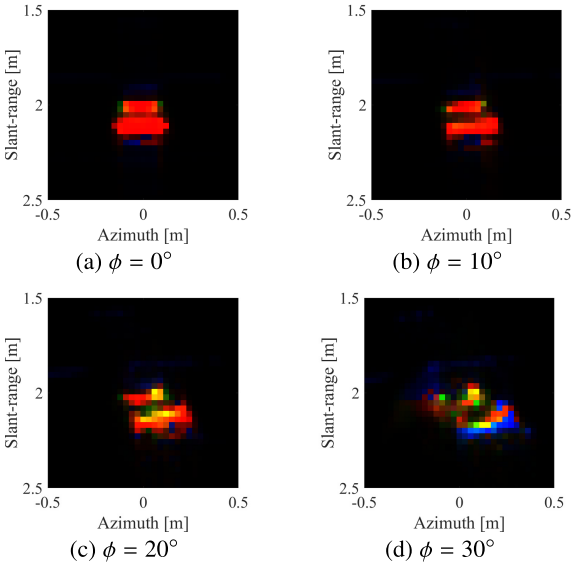

Fig. 7 RGB color composite image. $\theta = 25°$ (lit case).

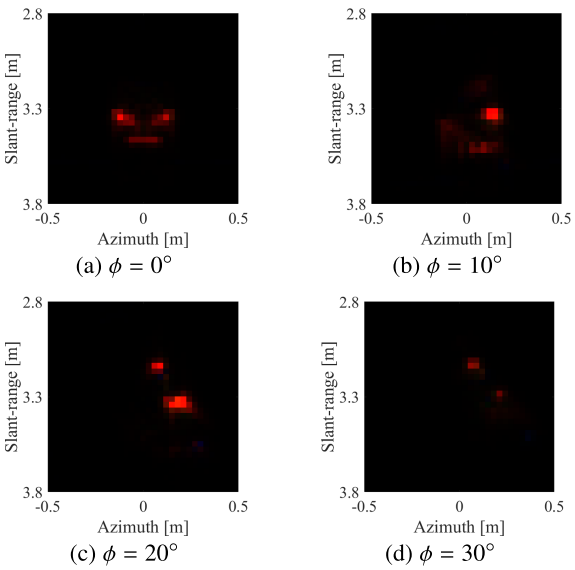

Fig. 8 RGB color composite image. $\theta = 55°$ (shadow case).

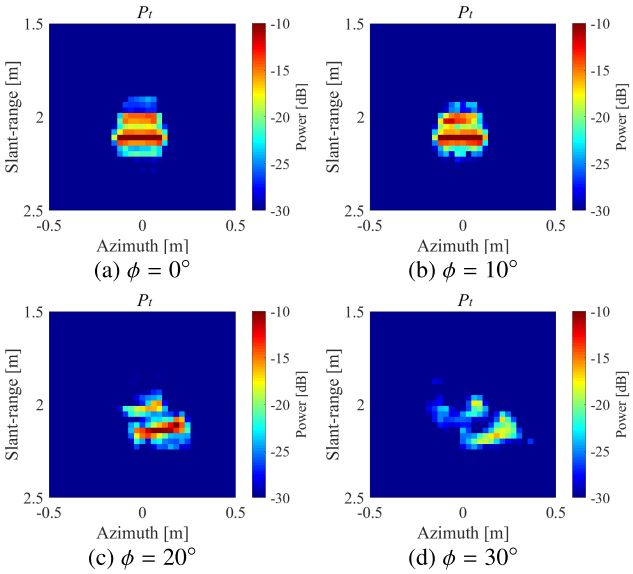

Fig. 9 SAR image of P_t. $\theta = 25°$ (lit case).

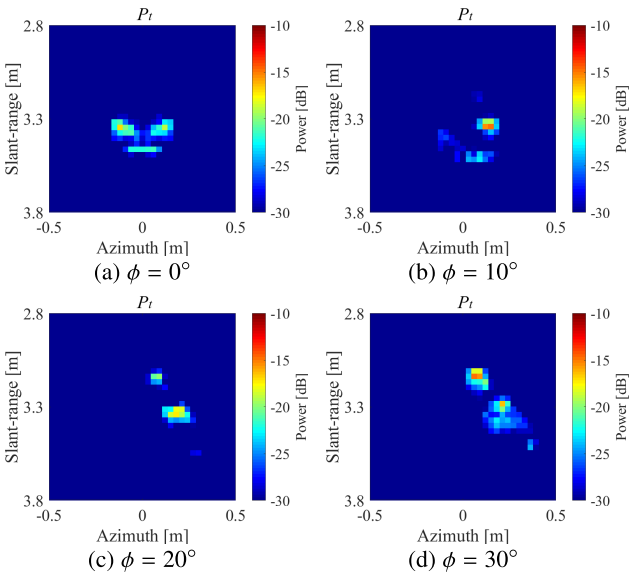

Fig. 10 SAR image of P_t. $\theta = 55°$ (shadow case).

VV co-pol ratio, as an additional polarimetric indicator for the distinction between "real" and "ghost" images.

4.2 Phase Difference of Co-Pol Ratio: χ

Figures 11 and 12 depict the SAR images of the phase of HH-VV co-pol ratio χ. The pixels with relatively strong total power P_t ($P_t > -30$ dB) are shown in the images. Also, the pixels with $P_t < -30$ dB are masked by black color. In comparison between the lit and shadow cases for each ϕ, it seems that the difference of χ of the building part is larger than that of the vehicle part when $\phi \leq 10°$.

Figure 13 shows the squint angle dependency of χ. In this figure, the phase is the mean value of χ calculated by the pixels of the vehicle and the buildings parts, after the OAC for the measured quad-polarimetric SAR data acquired in Sect. 3. Here the pixels of the vehicle and the buildings parts are extracted by considering the actual positions of the vehicle and the buildings models in the measurement. In the figure, the results for the lit ($\theta = 25°$) and shadow ($\theta = 55°$) cases are included. It is found from the comparison between the vehicle and buildings parts for the lit case that the phase of the vehicle part is larger than that of the building part. This tendency can be clearly observed for the shadow case. So, in addition to the information of P_d, by making use of this feature of χ, it may be possible to distinguish vehicle from buildings, and extract the vehicle shadowed by the buildings.

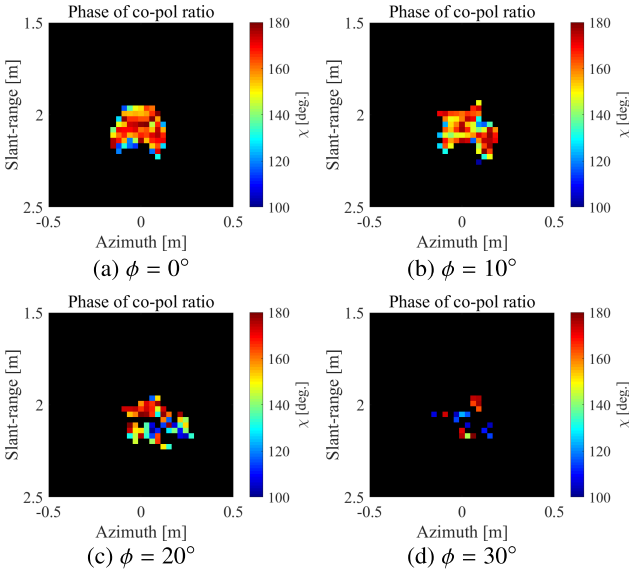

Fig. 11 Phase of co-pol ratio. $\theta = 25°$ (lit case).

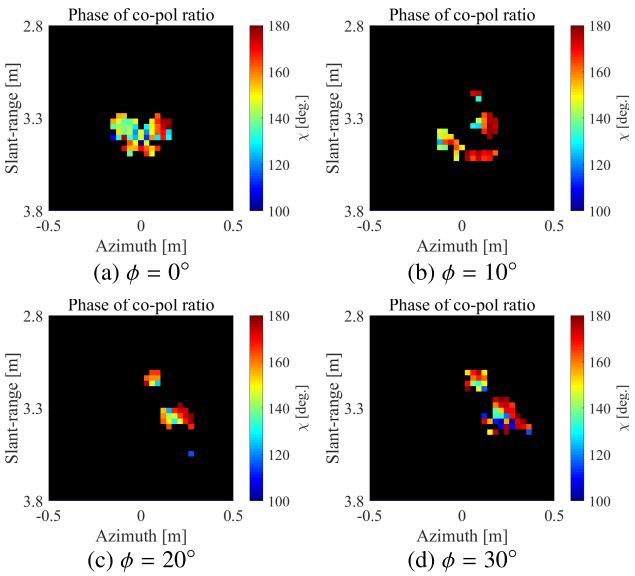

Fig. 12 Phase of co-pol ratio. $\theta = 55°$ (shadow case).

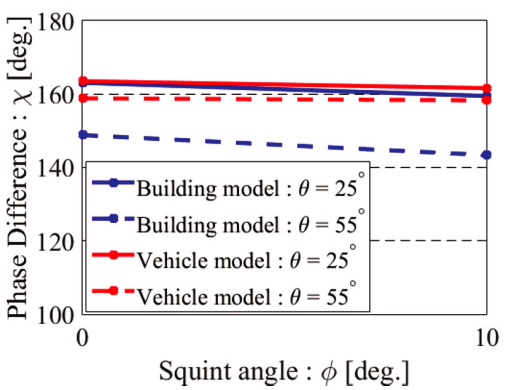

Fig. 13 Phase behavior of co-pol ratio for vehicle and building.

5. Vehicle Detection Algorithm in Flooded Urban Area

In this section, we shall propose a simple vehicle detection algorithm using quad-polarimetric SAR data, by considering the analysis results discussed in the previous section.

Figure 14 shows the flowchart of the proposed algorithm. In the algorithm, we firstly use the double-bounce scattering P_d obtained by the four-component decomposition to judge whether or not the pixels considered are in urban area. Secondly, we use the phase of HH-VV co-pol ratio, χ, to carry out the distinction between the vehicle and the building. Finally, we estimate "real" vehicle position, by using the phase difference between $\chi_{vehicle}$ and $\chi_{building}$, *i.e.* $\chi_{difference} = |\chi_{vehicle} - \chi_{building}|$, where $\chi_{vehicle}$ is χ for the pixels judged as vehicle, and $\chi_{building}$ is χ for the pixels eval-

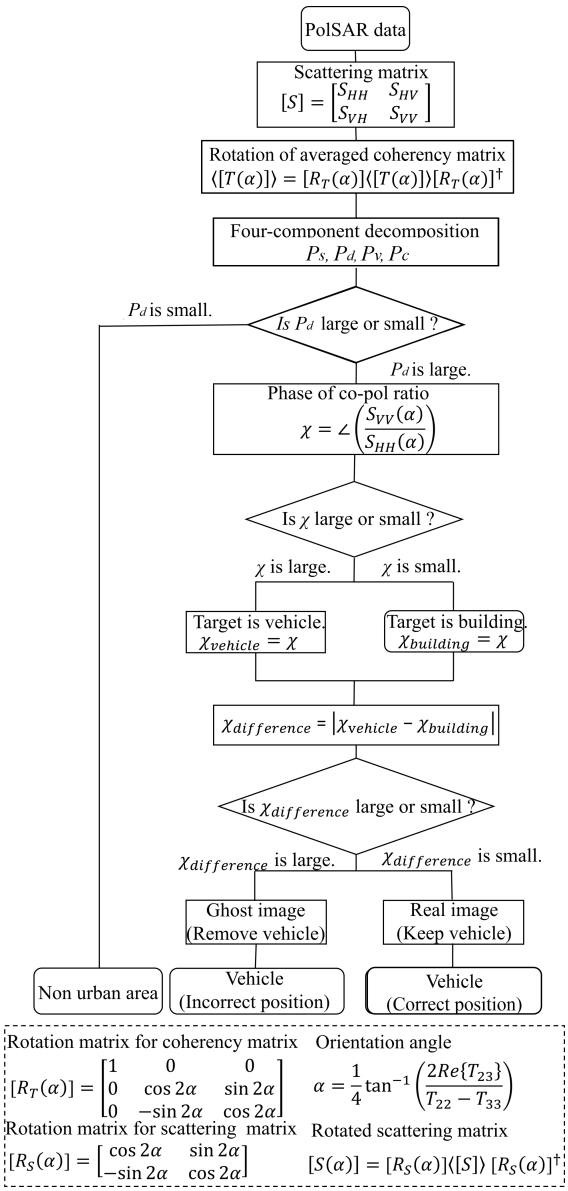

Fig. 14 Flowchart of the vehicle detection algorithm.

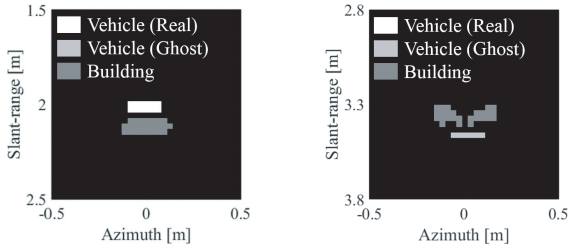

(a) $\theta = 25°$ (b) $\theta = 55°$

Fig. 15 Vehicle detection result. $\phi = 0°, \xi = 0°$.

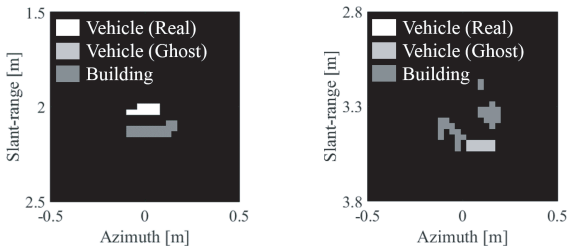

(a) $\theta = 25°$ (b) $\theta = 55°$

Fig. 16 Vehicle detection result. $\phi = 10°, \xi = 0°$.

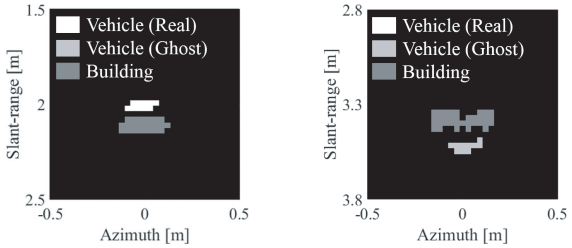

(a) $\theta = 25°$ (b) $\theta = 55°$

Fig. 17 Vehicle detection result. $\phi = 0°, \xi = 10°$.

uated as building. If $\chi_{vehicle}$ is close to $\chi_{building}$, *i.e.* $\chi_{difference}$ is small, then the pixels are considered as "real" image. So they provide us with correct position of the vehicle. On the other hand, when $\chi_{vehicle}$ is apart from $\chi_{building}$, *i.e.* $\chi_{difference}$ is relatively large, the pixels are considered as "ghost". For such case, the "ghost" pixels should be removed or handled with the utmost care in the final SAR image, to prevent the wrong estimation of the vehicle position.

5.1 Verification of the Accuracy of the Proposed Algorithm

In this subsection, we verify accuracy of the proposed algorithm by applying it to the quad-polarimetric SAR data obtained by the measurement in Sect. 3.

Figure 15 shows the vehicle detection result estimated by the proposed algorithm when both the building and the vehicle are normally aligned to radar direction ($\phi = 0°, \xi = 0°$). Here, the thresholds for judging whether P_d is large or small are -11 dB in lit case and -20 dB in shadow case. The mean values of χ obtained by the pixels of the manmade objects (the vehicle and buildings parts) are utilized as the thresholds for judging whether χ is large or small. Also, the threshold for $\chi_{difference}$ is here set as 9°. In the figure, 'white' and 'light gray' are painted for the pixels judged as 'vehicle', whereas 'gray' is for those as 'building'. Now please take a notice that the contribution of the building at the near side is not depicted in each image, since no double-bounce scattering (no strong scattered power) is generated by the building (See Figs. 2 and 6). It is found from the result of Fig. 15 (a) for the lit case ($\theta = 25°$) that the pixels with "white" color show right position of the vehicle model. On the other hand, for the shadow case of Fig. 15 (b) ($\theta = 55°$), the 'light gray color' pixels indicating the vehicle are observed at the wrong position behind the"gray" color pixels indicating the building at the far side. They are considered as "ghost" image of the vehicle.

Figure 16 presents the vehicle detection result when the building is obliquely oriented to the radar direction as $\phi = 10°$. The alignment of the vehicle is normal to the direction as $\xi = 0°$. It is observed from the result that the correct judgment for estimating the right vehicle position is performed for both the lit (Fig. 16 (a)) and shadow (Fig. 16 (b)) cases.

Similarly, one can observe from Fig. 17 that the vehicle detection accuracy of the proposed algorithm is still high even when the vehicle is obliquely oriented to the radar direction as $\xi = 10°$.

6. Conclusion

In this paper, we proposed a simple algorithm for detecting a vehicle trapped in flooded urban area, by making use of quad-polarimetric SAR data. In the vehicle detection algorithm, the four-component decomposition and phase difference of HH-VV co-pol ratio were used. To acquire the quad-polarimetric SAR data, we carried out polarimetric scattering measurement for a simplified model of flooded urban area in anechoic chamber. It was found from the result of the PolSAR image analysis for the measurement data that the proposed algorithm is effective to detect a vehicle trapped in flooded area even when the vehicle is located at severe position shadowed by building and/or its alignment is oblique to the radar illumination direction.

In this paper, however, we could not determine the appropriate criteria to judge whether P_d is large or small, and χ is large or small, for any incidence and squint angles. In particular, the characteristics of χ was not clear even for relatively small variation of ϕ ($\phi < 10°$). So, to try to make clear the characteristics of χ and determine the criteria, we will examine polarimetric scattering features from the vehicle model based on computational electromagnetic analysis. Furthermore, we could not confirm the validity of the proposed algorithm for high resolution PolSAR data acquired by actual sensors (ALOS-2/PALSAR-2, Pi-SAR-L2, Pi-SAR2, and so forth), since we did not have good quad-polarimetric SAR data including any vehicles in flooded urban area. So, in the future work, we will manage to obtain some actual quad-polarimetric SAR data including similar

situation and verify the validity of the algorithm to them.

As a future work, to realize a robust algorithm for more realistic environment and find out additional polarimetric indicators to extract vehicles in urban areas, we will examine polarimetric scattering characteristics caused by complex dihedral structures in flooded urban areas including floating debris, rough water surface due to wind, and so on, by carrying out additional measurement and computational simulation for the complex models.

Acknowledgments

This work was partially supported by JSPS KAKENHI Grant Number JP16K01285, Grant-In-Aid for test and research from The Uchida Energy Science Promotion, Japan, and Grant-In-Aid for research and development from NAGAI N.S. Promotion Foundation for Science of Perception, Japan. The authors would like to thank the associate editor and anonymous reviewers for their valuable comments and suggestions.

References

[1] I.G. Cumming and F.H. Wong, Digital processing of Synthetic Aperture Radar Data, Artech House, 2005.
[2] Y. Yamaguchi, T. Moriyama, M. Ishido, and H. Yamada, "Four-component scattering model for polarimetric SAR image decomposition," IEEE Trans. Geosci. Remote Sens., vol.43, no.8, pp.1699–1701, Aug. 2005. DOI: 10.1109/TGRS.2005.852084
[3] Y. Yamaguchi, A. Sato, W.-M. Boerner, R. Sato, and H. Yamada, "Four-component scattering power decomposition with rotation of coherency matrix," IEEE Trans. Geosci. Remote Sens., vol.49, no.6, pp.2251–2258, June 2011. DOI: 10.1109/TGRS.2010.2099124
[4] Y. Yamaguchi, Radar Polarimetry from Basics to Applications: Radar Remote Sensing using Polarimetric Information, IEICE, 2007 (In Japanese).
[5] J.-S. Lee and E. Pottier, "Polarimetric Radar Imaging: From Basics to Applications," CRC Press, 2009.
[6] S.R. Cloude, "Polarisation: Applications in Remote Sensing," Oxford University Press, 2010. DOI: 10.1093/acprof:oso/9780199569731.001.0001
[7] J. van Zyl and Y. Kim, "Synthetic Aperture Radar Polarimetry," Wiley, 2010. DOI: 10.1002/9781118116104
[8] T. Ishikuro, R. Sato, Y. Yamaguchi, and H. Yamada, "Study on flooded damaged vehicle detection by quad-pol SAR data analysis in urban area," The papers of Technical Meeting on Electromagnetic Theory, IEE Japan, vol.EMT-17-137, pp.187–192, Nov. 2017.
[9] J.-S. Lee, D.L. Schuler, and T.L. Ainsworth, "Polarimetric SAR data compensation for terrain azimuth slope variation," IEEE Trans. Geosci. Remote Sens., vol.38, pp.2153–2163, 2000. DOI: 10.1109/36.868874
[10] H. Kimura, "Radar polarization orientation shifts in built-up areas," IEEE Geosci. Remote Sensing Letters, vol.5, no.2, pp.3050–3056, April 2008. DOI: 10.1109/LGRS.2008.915737

Takanori Ishikuro received B.E. and M.E. degrees in information engineering from Niigata University, Niigata, Japan, in 2016 and 2018, respectively. He was engaged in radar polarimetry.

Ryoichi Sato received the B.S., M.S. and Ph.D. degrees in electrical engineering from Chuo University, Tokyo, Japan, in 1992, 1994 and 1997,respectively. Since April 1997, he has been with the Faculty of Education, Niigata University, Japan, where he is currently a Professor. In 2002, he was a Research Scholar at Polytechnic University, Brooklyn, NY. He received the Young Scientist Paper Award of the 5th International Conference on Mathematical Methods in Electromagnetic Theory (MMET*94) in 1994, the Paper Presentation Award from the Institute of Electrical Engineers of Japan (IEEJ) in 2000, and the Best Poster Award of the 7th European Conference on Synthetic Aperture Radar (EUSAR 2008) in 2008. His current research interests are electromagnetic wave propagation, scattering and diffraction, and radar polarimetry. Dr. Sato is a member of the IEEE, and the IEE of Japan.

Yoshio Yamaguchi received the B.E. degree from Niigata University, Niigata, Japan, in 1976, and the M.E. and Dr-Eng. degrees from the Tokyo Institute of Technology, Tokyo, Japan, in 1978 and 1983, respectively. In 1978, he joined the Faculty of Engineering, Niigata University. He is a professor of Niigata University. From 1988 to 1989, he was a Research Associate with the University of Illinois at Chicago, Chicago, IL, USA. His research interests include radar polarimetry, microwave scattering, decomposition, and imaging. Dr. Yamaguchi is a Fellow of IEICE and IEEE, and recipient of the 2008 IEEE Geoscience and Remote Sensing Society Education Award and 2018 IEEE GRSS Distinguished Achievement Award.

Hiroyoshi Yamada received the B.E., M.E. and Dr.Eng. degrees in electronic engineering from Hokkaido University, Sapporo, Japan, in 1988, 1990 and 1993, respectively. In 1993, he joined the Faculty of Engineering, Niigata University, where he is a professor. From 2000 to 2001, he was a Visiting Scientist at the Jet Propulsion Laboratory, California Institute of Technology, Pasadena. His current interests include superresolution techniques, array signal processing, and microwave remote sensing and imaging. Dr. Yamada received the Young Engineer Award of IEEE AP-S Japan Chapter in 1992, the Young Engineer Award of IEICE Japan in 1999, the Kiyasu-Zenichi Award and the Best Paper Award of IEICE both in 2010, and the Best Tutorial Paper Award from Comm. Soc. of IEICE in 2010. Dr. Yamada is a member of the IEEE.